WILEY-VCH

Research Article

Artificial Lithium Channels

DOI: 10.1002/anie.200((will be filled in by the editorial staff))

Sulfur-Containing Foldamer-Based Artificial Lithium Channels

*Jie Shen, Deepa R, Zhongyan Li, Hyeonji Oh, Harekrushna Behera, Himanshu Joshi, Manish Kumar, Aleksei Aksimentiev and Huaqiang Zeng**

Abstract: *Unlike many other biologically relevant ions (Na^+, K^+, Ca^{2+}, Cl^-, etc) and protons, whose cellular concentrations are closely regulated by highly selective channel proteins, Li^+ ion is unusual in that its concentration is well tolerated over many orders of magnitude and that no lithium-specific channel proteins have so far been identified. While one naturally evolved primary pathway for Li^+ ions to traverse across the cell membrane is through sodium channels by competing with Na^+ ions, highly sought-after artificial lithium-transporting channels remain a major challenge to develop. Here we show that sulfur-containing organic nanotubes derived from intramolecularly H-bonded helically folded aromatic foldamers of 3.6 Å in hollow cavity diameter could facilitate highly selective and efficient transmembrane transport of Li^+ ions, with high transport selectivity factors of 15.3 and 19.9 over Na^+ and K^+ ions, respectively.*

Introduction

In addition to its usefulness in reducing suicide attempts and in treating unipolar depression, some cancers, and neurodegenerative diseases such as Alzheimer's disease,[1a, 1b] the mood-stabilizing Li^+ ion also remains the first line therapeutic agent for long-term management of bipolar disorder, which affects nearly 2.8% of the adult U.S. population[1c] with cost of $195 billion for 2018 in the U.S. alone.[1d] While Li^+ ion exerts many and varied physiological and biochemical effects via mechanisms mostly still poorly understood,[1a] one major drawback of lithium therapy of bipolar disorder is its narrow therapeutic window of 0.6 - 1.2 mM above which severe side effects (cognitive impairment, hypothyroidism, renal failure, tremors, etc) may result.[1e] Further, low membrane penetration rate of the Li^+ ion, lack of Li^+-specific channel proteins[1a] and a need to use sodium channel for facilitated Li^+ transport[1f,1g] all might account for why an effective lithium therapy calls for a high minimum concentration of 0.6 mM from different aspects. Hence, artificial lithium-transporting channels might shift the therapeutic window to a lower concentration regime by facilitating transmembrane transport of Li^+, concurrently offering enhanced therapeutic outcomes and reduced side effects. Given that there are 5000 times more Li^+ in the seawater than on land sources,[2a] these artificial lithium channels may also radically transform the technology for lithium mining from the salt lakes or seawater.[2b] Undesirably, Li^+ ion is the most highly polarized and has the highest dehydration energy among the five alkali metal ions, making high transport selectivity against other alkali metal ions exceptionally difficult to attain. Despite that intensive explorations over the past four decades[3] have culminated in a number of artificial channels capable of mediating selective cross-membrane transport of K^+,[4] Na^+,[5] Cl^-,[6] I^-,[7] ClO_4^-,[8] H^+,[9] and H_2O,[10] research endeavours over the past years have not been very successful in creating artificial lithium channels, with just one very recent example reported by Dong et al in 2023.[11]

Pioneered by Hamilton,[12a] Lehn[12b] and Gong[12c] in 1990s, intramolecularly H-bonded aromatic amide foldamers (HAAFs) make an intelligent use of intramolecular multiple-centre H-bonding forces to fold a single amide bond-linked molecular backboxne predominantly into a highly rigid helical architecture,[12d-g] which can remain stably folded even in water.[12h] Additionally stabilized by extensive π-π stacking forces, these HAAFs enclose a hollow cavity of 2.8 Å[10d] to 30 Å[12i] in diameter. What is intrinsic to these HAAFs is high predictability in both the helical structure and the hollow cavity size encoded into their constituent helicity codons.[12g] This unusual structural uniqueness renders the cavity size highly designable and the guest-binding properties more or less inferable from the functional groups of the helicity codons.[12d-g] Nevertheless, their functional investigations within the context of lipid membrane have been greatly hampered by synthetic difficulties in preparing long HAAFs of > 1 nm in nanotubular length, due to the H-bonding-rigidified aromatic backbone that bestows the repeating units with low reactivities. To get around the synthetically challenging, time-consuming and resource-intensive multi-step synthesis,[13a,13b] one-pot

[*] Prof. Dr. J. Shen, Ms. Z. Li and Prof. Dr. H. Zeng
College of Chemistry
Fuzhou University
Fuzhou, Fujian 350116, China
E-mail: hqzeng@fzu.edu.cn

Ms. D. R. and Dr. H. Joshi
Department of BioTechnology
Indian Institute of Technology Hyderabad
Kandi, Sangareddy 502285, Telangana, India

Ms. H. Oh, Mr. H. Behera and Prof. Dr. M. Kumar
McKetta Department of Chemical Engineering
The University of Texas at Austin
Austin, TX 78712, USA

Prof. Dr. A. Aksimentiev
Department of Physics and Beckman Institute for Advanced Science and Technology
University of Illinois at Urbana-Champaign
Urbana, IL 61820, USA

Supporting information for this article is available on the WWW under: http://www.angewandte.org or from the author.

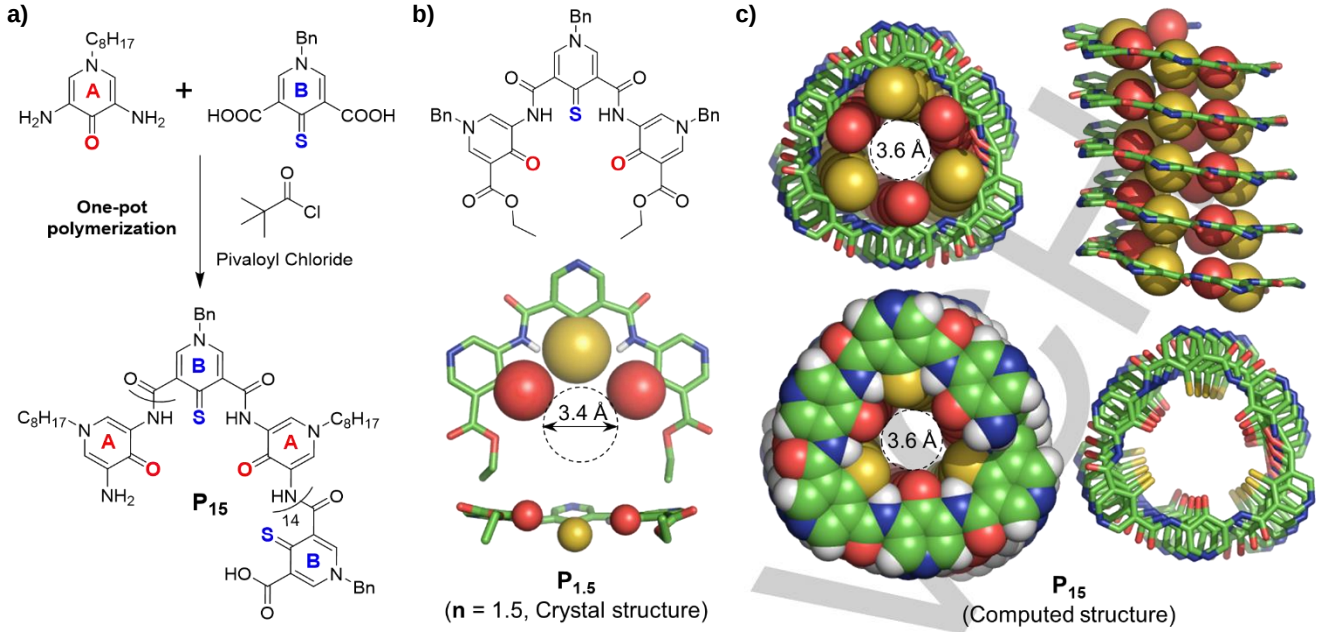

Figure 1. Molecular design and structure of HAAF-derived channels **P_{15}**. a) Structure of artificial lithium channels **P_{15}** readily made from pyridone (**A** unit) and thio-pyridone (**B** unit) through the pivaloyl chloride-mediated one-pot polymerization at 67% yield. b) Crystal structure of a short oligomer molecule **$P_{1.5}$** made up of two **A** units and one **B** unit (CCDC2181960), revealing an H-bonding-induced crescent-shaped structure that encloses an internal cavity of about 3.4 Å in diameter after subtracting the van der Waals radii of the O- and S-atoms. c) Molecular dynamics-optimized backbone scaffold of **P_{15}**, illustrating excellent structural resemblance to **$P_{1.5}$** that suggests about three repeating **AB** units per helical turn and manifests an electron-rich interior decorated by the O- and S-atoms for cation transport. In b), the exterior benzyl (Bn) groups were removed from the crystal structure of **$P_{1.5}$** for clarity of view.

polymerization strategy conceived to be the most atomically economic has been adopted by several researchers, currently producing only short polymeric HAAFs of ≤ 1.1 nm from unprotected repeating units.[13c]

Envisioning an entirely new membrane-related functional space, we recently started developing one-pot polymerization reagents for generating HAAF-based long organic nanotubes.[9a,14] Out of 20 amide coupling agents tested, we identified phosphoryl chloride and PyBOP as the only reagents that respectively generate pyridine-derived nanotubes of ~ 2.8 nm in length and 2.8 Å in cavity diameter as proton/water channels[14] and pyridine/pyridone-based nanotubes of ~ 3.4 nm in length and 3.0 Å in cavity diameter as highly selective proton channels.[9a] Through our continuing investigation, here we show that pivaloyl chloride[15] could serve as a third mild coupling reagent, enabling facile one-pot construction of sufficiently long **P_{15}** from pyridone (**A**) and thio-pyridone (**B**) units (Figure 1a). Surprisingly yet significantly, the relatively short channel **P_{15}** (~ 2.1 nm in average nanotube length inclusive of the atomic thickness of the end units and ~ 3.6 Å in hollow cavity diameter) not only transports Li^+ via a channel mechanism but also transports it with high efficiency (γ_{Li^+} = 18.4 ± 0.4 pS that is comparable to γ_{K^+} = 23.2 ± 0.4 pS displayed by gramicidin A[4b]) and high transport selectivity factors of 15.3 and 19.9 against Na^+ and K^+ ions, respectively.

Results and Discussion

Synthetic construction and structural features of P_{15}

Aromatic foldamer-based **AB** type nanotubes **P_n**, having its hollow cavity fully decorated by electron-rich O- and S-atoms, have never been reported before. Such type of nanotubes will function as cation-transporting channels when embedded within the lipid bilayer, possibly exhibiting some sort of cation transport selectivity.

To elucidate the key structural features of **P_{15}**, we determined the crystal structure of a short oligomer molecule **$P_{1.5}$** (Figure 1b). In accordance with our design, the crystal structure shows a crescent-shaped geometry rigidified by four intramolecular H-bonds formed between amide H-atoms and pyridone S- and O-atoms. For one, the structure of **$P_{1.5}$** validates the design principle that applies the relatively weaker intramolecular H-bond of N-H•••S=C type[16] to induce and maintain a curved conformation, which is further enforced by the repulsive S•••O forces. For the other, structural extrapolation based on **$P_{1.5}$** suggests an enclosed electron-rich cavity of ~ 3.4 Å in diameter after subtracting the van der Waals radii of the S- and O-atoms, and three repeating **AB** type units per helical turn.

Prompted by the designed and experimentally verified folded structure of **$P_{1.5}$**, we started searching new one-pot polymerization argents for mild and efficient generation of longer versions of **$P_{1.5}$** (Scheme S1), with the average molecular weight (M_n) measured using the gel permeation chromatography (GPC) method (Figures S3 and S4). While varying coupling reagents (PyBOP, HATU, HBTU, BOP, etc) produce highly soluble products, having a GPC-derived M_n of < 3000 Da (Tables 1 and S3), the pivaloyl chloride-mediated

Table 1. Molecular weights (M_n, Da) of polymers $\mathbf{P_n}$ produced using different types of coupling agents.[a]

	Pivaloyl Chloride	HATU, HBTU, BOP, PyBOP
M_n	7599[b]	< 3000

[a] M_n was determined using GPC. [b] This Mn value corresponds to $\mathbf{P_{15}}$ having 15.45 **AB** repeating units and an average nanotube length of 2.1 nm.

one-pot copolymerization of **A** and **B** units generates longer $\mathbf{P_n}$, having M_n of 7599 Da that compares well with the NMR-derived molecular weight (Scheme S2 and Figure S2), at 67% yield (Figure 1a). Given a molecular weight of 489.63 for the **AB** repeating unit, this M_n of 7599 Da corresponds to 15.45 **AB** units contained in $\mathbf{P_n}$, which was hence named as $\mathbf{P_{15}}$. Subsequent computation on $\mathbf{P_{15}}$ using a molecular dynamics approach yields a hollow cavity of 3.6 Å in diameter enclosed by helically aligned O- and S-atoms and ~ 3.02 **AB** units per helical turn (Figure 1c), closely resembling those structural features seen in the crystal structure of $\mathbf{P_{1.5}}$. By including the atomic thickness of the end units, $\mathbf{P_{15}}$ measures 2.1 nm long.

$\mathbf{P_{15}}$ selectively transports lithium ions

A fluorescence-based HPTS assay, having intravesicularly encapsulated pH-sensitive HPTS dye and a proton gradient of pH 7 to 8 across the membrane, was applied to investigate the ion transport activity of polymeric HAAFs. With polymers set at 0.19 μg/mL (e.g., 0.25 μM for $\mathbf{P_{15}}$), we obtained the fractional ion transport activities of 8.0% to 15.5% for short HAAFs of M_n < 3000 Da, which was generated using HATU, HBTU, BOP and PyBOP, and the highest activity of 71.6% for $\mathbf{P_{15}}$, which was generated using pivaloyl chloride (Figure 2a). These results confirm pivaloyl chloride as the best one-pot polymerization reagent among the five tested, giving rise to the most active channel $\mathbf{P_{15}}$ of 2.1 nm.

By varying extravesicular alkali metal chlorides and with [$\mathbf{P_{15}}$] = 0.25 μM, we obtained fractional ion transport activities of 6.4%, 6.1%, 6.2% and 5.4% for NaCl, KCl, RbCl and CsCl after normalization based on their respective background values of 9.1, 4.9%, 6.6%, 2.0% and 3.8% (Figures 2b and S5a). These comparative activity data unambiguously demonstrate that $\mathbf{P_{15}}$ transports Li^+ with high rejection of Na^+, K^+, Rb^+ and Cs^+ ions.

A weak ion transport activity of 6.4% for NaCl additionally reveals low permeability of both protons and Cl^- anions through $\mathbf{P_{15}}$.This is because a channel that is mostly impermeable to Na^+ ions but readily mediates a rapid efflux of protons requires a passive influx of Na^+ ions for charge neutralization, causing large changes in the HPTS fluorescence intensity and the corresponding changes in fractional ion transport activity far beyond 6.4%. With the same reasoning, a channel-induced efflux of Cl^- anions will be accompanied by a proton efflux, leading to changes in transport activity much greater than 6.4%.

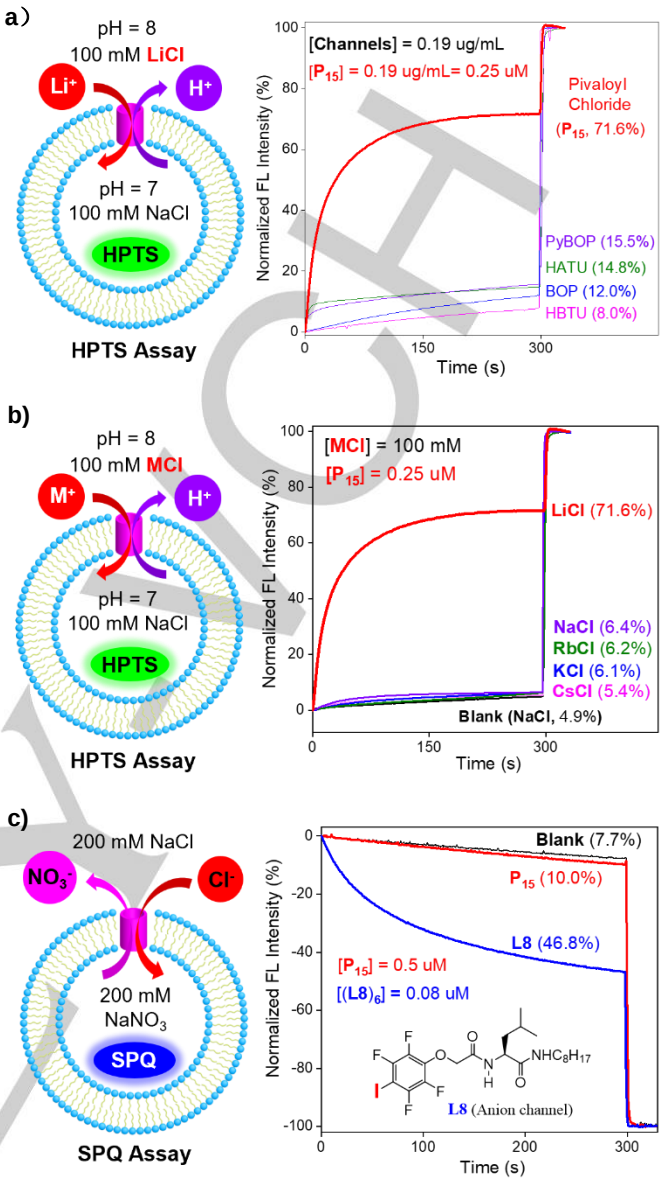

Figure 2. Channel $\mathbf{P_{15}}$ of 2.1 nm in nanotube length selectively transports lithium ions. a) Incorporating a pH-sensitive HPTS dye, the HPTS fluorescence assay data establish the pivaloyl chloride as the best one-pot polymerization reagent compared to others tested (HATU, HBTU, BOP and PyBOP), generating the most active channel $\mathbf{P_{15}}$ of 2.1 nm that exhibits a fractional lithium transport activity of 71.6%. b) With the extravesicular region varied to have 100 mM MCl, the HPTS assay data demonstrate highly selective transport of Li^+ by $\mathbf{P_{15}}$ while rejecting Cs^+, Rb^+, Na^+, K^+, Cl^- and H^+. c) Incorporating a chloride-sensitive SPQ dye, the SPQ assay data confirm the inability of $\mathbf{P_{15}}$ to transport Cl^- ions. It has been demonstrated that six to seven molecules of **L8** self-assemble to form H-bonded ensembles of ≥ 3 nm in length to serve as efficient anion channels.[6f] [Total lipid] = 50 μM. SPQ = 6-Methoxy-N-(3-sulfopropyl)quinolinium.

The low permeability to anions can be further established using the SPQ assay (Figure 2c). This assay relies on the ability of Cl^- anions to quench the fluorescence of SPQ dye.

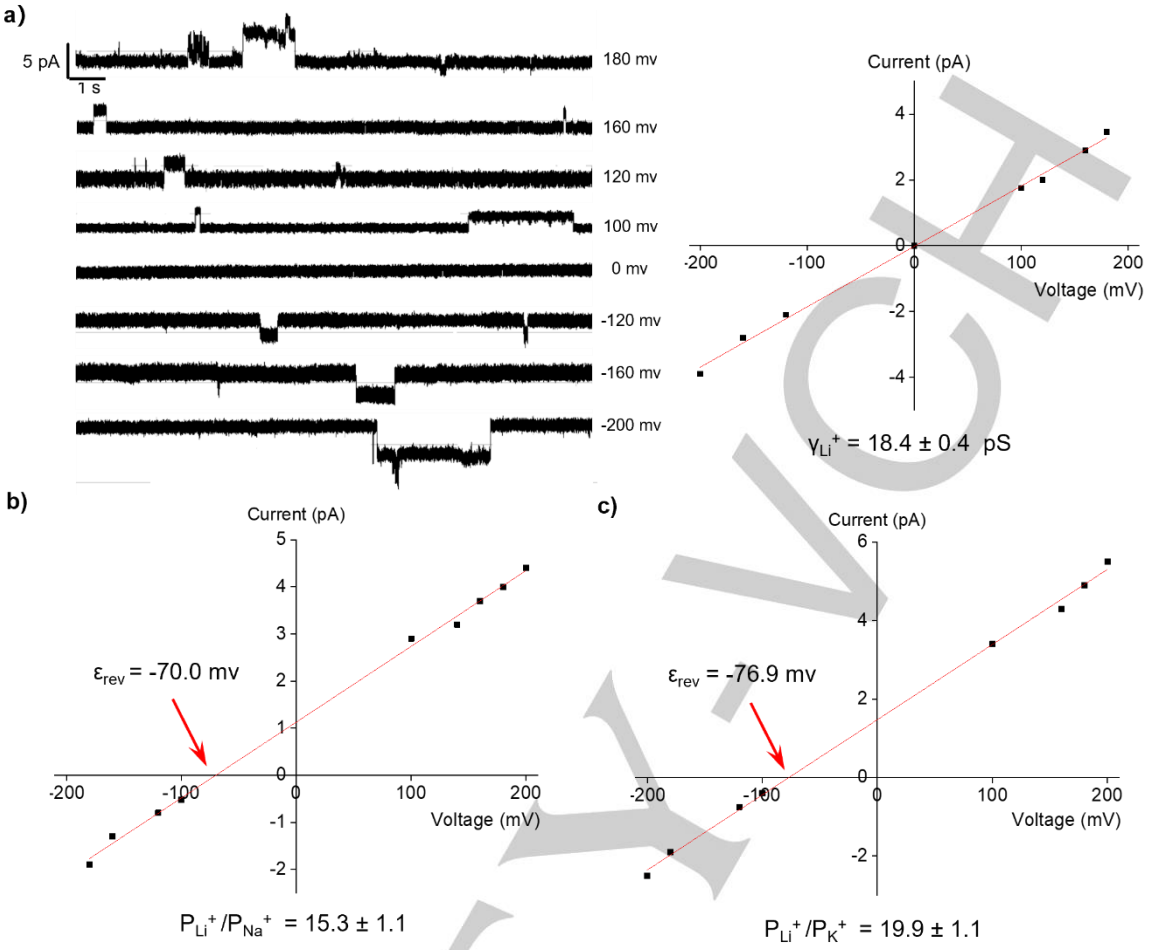

Figure 3. Current traces and current-voltage (I-V) curves for P_{15} recorded at the single channel level in a lipid bilayer for determining lithium conduction rate (γ_{Li+}) and lithium transport selectivity. a) Single channel current traces and I-V curve (*cis* chamber = *trans* chamber = 1 M LiCl) from which the γ_{H+} value for **P_{15}** was determined to be 18.4 ± 0.4 pS. b) I-V curve (*cis* chamber = 1 M LiCl, *trans* chamber = 1 M NaCl) from which Li^+/Na^+ (P_{Li+}/P_{Na+}) selectivity value for **P_{15}** was determined to be 15.3 ± 1.1, c) I-V curve (*cis* chamber = 1 M LiCl, *trans* chamber = 1 M KCl) from which Li^+/K^+ (P_{Li+}/P_{K+}) selectivity value for **P_{15}** was determined to be 19.9 ± 1.1. In **a**, γ_{H+} was obtained by fitting the I-V curve using a linear equation of y = a + b*x where slope b is γ_{H+} in the unit of nS. In **b** and **c**, the permeability ratio (P_{Li+}/P_{M+}) was calculated using a simplified Goldman−Hodgkin−Katz equation $\varepsilon_{rev} = RT/F \times \ln(P_M^+/P_{Li}^+)$, where R = universal gas constant (8.314 $J \bullet K^{-1} \bullet mol^{-1}$), T = 300 K, F = Faraday's constant (96485 $C \bullet mol^{-1}$), and *P* is the permeability of the ions.

Therefore, while a chloride-transporting channel (**L8**)$_6$[6f] allows for cross-membrane exchanges between Cl^- with nitrate anions, leading to time-dependent quenching of SPQ, **P_{15}**, which is unable to induce a significant influx of Cl^-, exerts little influence on the fluorescence intensity of SPQ even at 0.5 μM, a concentration six times that of (**L8**)$_6$.

Using the Hill Analysis, the EC_{50} value at which **P_{15}** achieves 50% fractional ion transport activity was determined to be 0.16 μM or 0.32 mol% relative to lipid (Figure S5b), confirming high Li^+ transport activity.

P_{15} transports lithium ions through a channel mechanism with high selectivity

With an appreciable nanotube length of 2.1 nm and an electron-rich cavity of 3.6 Å in diameter, it is highly likely that **P_{15}** functions as a single channel for Li^+ transport. Planar lipid bilayer experiments were then conducted for **P_{15}** in symmetric baths (*cis* chamber = *trans* chamber = 1 M LiCl, Figure S6). Except for 180 mV, the recorded current traces at all other voltages (–200 mV to 160 mV) exhibit well-defined single channel current traces (Figure 3a), confirming the single channel behaviour by **P_{15}**. Based on the plotted current *vs* voltage (I-V) curve, a linear regression analysis using equation y = a + b*x yields lithium conduction rate (γ_{Li}^+) of 18.4 ± 0.4 pS (Figure 3a). Considering the γ_{K}^+ value of 23.2 ± 0.4 pS for gramicidin A (gA) recently determined by us,[4b] **P_{15}** efficiently transports Li^+ ions at ultrafast rate 80% as fast as gA transports K^+ ions.

Among the low transportable ions (Na^+, K^+, Rb^+ and Cs^+, Figure 2a), biologically relevant Na^+ and K^+ ions were studied further. To quantify Li^+/Na^+ transport selectivity, the same set of planar lipid bilayer experiments was subsequently conducted in unsymmetrical baths (*cis* chamber = 1.0 M LiCl and *trans* chamber = 1.0 M NaCl). Based on the recorded single channel current traces (Figure S7) that validate a single

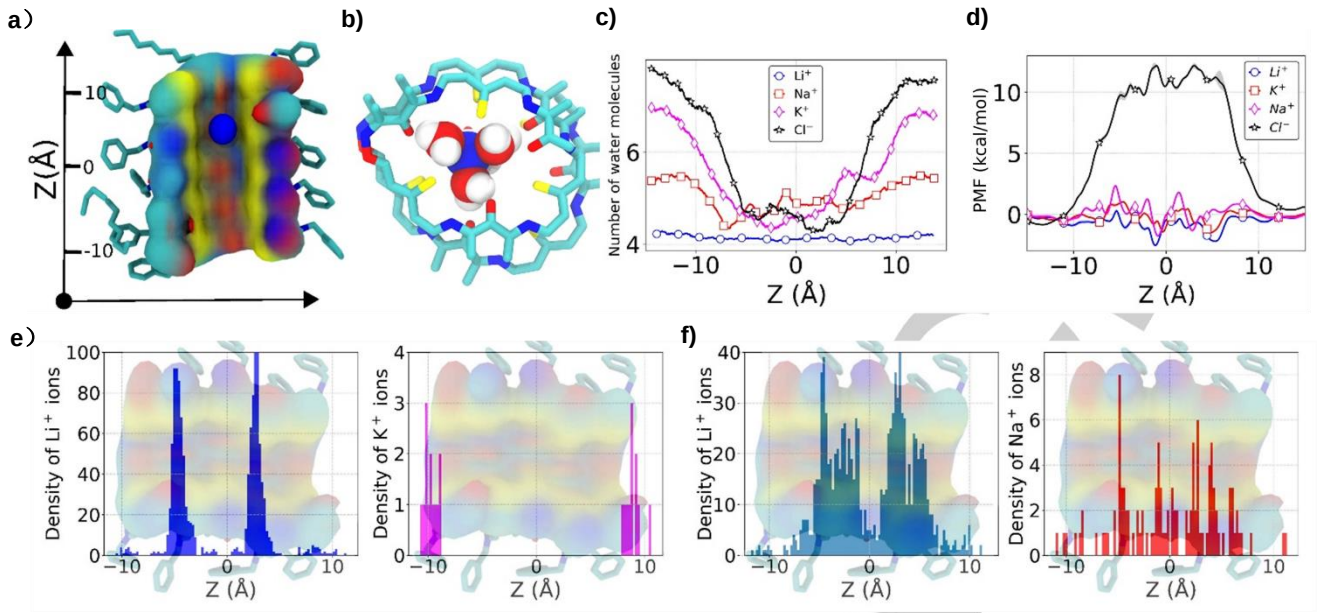

Figure 4. All-atom MD simulations of ion permeation through the **P_{15}** channel. a) A representative snapshot of the simulated system showing the cut-away side view of **P_{15}** channel (water and ions are not shown). b) Top view of the Li^+ ion (blue) and its first hydration shell, illustrating the H-bonds formed between water H-atoms and the channel's O-atoms. c) The number of water molecules in the first hydration shell of the ion as a function of its distance from the center of **P_{15}** as the ion translocates through the channel. d) Free energy profile (PMFs) of the Li^+, Na^+, K^+ and Cl^- ions as a function of the distance from the center of **P_{15}** along the channel axis computed using the REUS method. e) Average densities of Li^+ and K^+ ions in the presence of 0.5 M KCl as a function of their distance from the channel center along the ***z*** axis. f) Average densities of Li^+ and Na^+ ions in the presence of 0.5 M NaCl as a function of their distance from the channel center along the ***z*** axis. The transparent background images in both panels e) and f) show the cut-away views of the channel, and plotted ion densities were averaged for the last 0.8 μs restrain free equilibrium MD simulation trajectories.

channel conduction mechanism, a I-V curve can be plotted, giving rise to a reverse potential value of -70.0 mV (ε_{rev}, Figure 3b). Using a simplified Goldman−Hodgkin−Katz equation (ε_{rev} = RT/F × ln(P_{Na^+}/P_{Li^+}), Li^+/Na^+ transport selectivity is calculated to be 15.3.

Similarly, a high Li^+/K^+ transport selectivity factor of 19.9 can be obtained from the determined ε_{rev} value of -76.9 mv (Figures 3c and S8).

Through the investigation of four artificial K^+-selective channels **5Fn** (n = 8 - 14),[4h] we recently found an interesting correlation between the binding constant (K_a) and transport selectivity. Having K^+/Na^+ transport selectivity factors of 9.8 - 20.1, **5Fn** all display a higher K_a (Na^+) value that is 3 - 5 times that of K_a (K^+). With the highest K^+/Na^+ selectivity factor of 20.1, **5F14**'s K_a (K^+) of 0.82 × 10^3 M^{-1} is three times as weak as K_a (Na^+) of 2.46 × 10^3 M^{-1}. Inspired by this observation, we have also determined the K_a values of **$P_{1.5}$** toward alkali metal ions (Table S2). The determined K_a values similarly point to the same trend as that of **5Fn** series. That is, **$P_{1.5}$** binds Li^+ ion (K_a = 0.89 × 10^3 M^{-1}) about three times weaker than Na^+ (K_a = 3.90 × 10^3 M^{-1}) and K^+ (K_a = 4.00 × 10^3 M^{-1}) ions, a trend that is in line with the fact that **P_{15}** selectively transports Li^+ ions.

Computational insights into the selective lithium passage through P_{15}

To visualize and understand the molecular level structure and Li^+ ion selectivity of the **P_{15}** channel, we performed all-atom simulations using NAMD2 program.[17a] Based on the crystal structure of **$P_{1.5}$** (Figure 1b), we built an all-atom model of the **P_{15}** channel (Figures 1c, 4a and S7a-b as well as Supplementary Video SV1) and solvated it in a 0.5 M aqueous solution of LiCl. Two simulation systems were created by adding 0.5 M KCl (System 1) or 0.5 M NaCl (System 2), respectively. The overall structure and the diameter (~ 3.6 Å) of **P_{15}** largely remain unchanged at the end of 1 μs long equilibrium simulations without any restraints (Figure S9c-d and Supplementary Video SV2).

Owing to its smallest hydration shell comprising 4 water molecules[17b] as compared to the other alkali metal ions, the hydrated Li^+ ion fits well inside the **P_{15}** channel (Figures 4b and S10). Within the first few nanoseconds of the MD simulations in both Systems 1 and 2, we observed that Li^+ ions readily enter **P_{15}** and that there are always two Li^+ ions residing inside **P_{15}** during the whole 1 μs long MD simulations (Figure S9e). In contrast, no Cl^- ions ever enter the channel. Occasionally, some Na^+ ions also entered the channel (Figure S9f). The average density of Li^+ ions measured inside the channel is far more than one order of magnitude higher than both Na^+ and K^+ ions (Figure 4e-f). Interestingly in the presence of KCl, the hydrated Li^+ ions stabilized the channel structure slightly better than NaCl system via the formation of long-lasting H-bonds between the H-atoms of water molecules and O-atoms from the channel wall (Figure 4b-c). The average number of water molecules present inside the channel turns out to be ~ 15 and 19 in system 1 and system 2 (Figure S11), respectively.

By forming H-bonds with the inner walls of **P_{15}** (Figure S12), the water molecules present inside the channel compensate the lost hydrogen bonds due to confinement from the narrow cavity. Li^+ ions inside the channel appear to form a weak hexagonal coordination with the sulfur atoms that decorate the channel wall, with average distance of about 5 Å (Figure S11). Thus, our equilibrium simulations strongly suggest that the small pore size of **P_{15}** appears to be ideal fit for permeating the Li^+ ions, a transport process assisted by the surrounded water molecules and sulfur atoms, while sterically excluding the Cl^- ions and the other larger alkali metal ions such as Na^+ and K^+ ions.

To further investigate the Li^+ selectivity, we have performed free energy calculations using the replica exchange umbrella sampling (REUS) method[15c] (Figure 4d). The computed high free energy barrier for Cl^- ions certainly prevents these anions from entering **P_{15}**. Corroborated further by the "knock-on" mechanism (Supplementary Video SV2), the consistently more negative free energies of Li^+ ions as compared to those for the K^+ and Na^+ ions explain the highly selective permeation of Li^+ ions through **P_{15}**.

Conclusion

To summarize, we have demonstrated here that sulfur-containing helically folded aromatic foldamers, possessing helically arranged O-atoms and S-atoms along the hollow cavity wall of ~ 3.6 Å in diameter, can serve as artificial lithium channels, with high preference of Li^+ ions over other alkali metal ions. In particular, Li^+/Na^+ and Li^+/K^+ selectivity factors reach 15.3 and 19.9, respectively. Given the crucial roles lithium ions play in treating bipolar disorder and unipolar depression[1a,1c,1e] as well as in the lithium-ion battery, this novel class of artificial lithium channels and their further optimized analogues may find interesting uses as medical agents or in fabricating artificial lithium channel-based membrane for lithium mining from salt lakes or seawater.[2b]

Acknowledgements

This work is supported by the National Natural Science Foundation of China (NO. 22271049), start-up grant from Fuzhou University, the US National Science Foundation under grants of DMR-1827346, CBET 1946392 and CBET 1952295, the National Institutes of Health under grant of P41-GM104601 and Science and Engineering Research Board (India) grant SRG/2022/002109 and DST Inspire faculty fellowship IFA20-PH-256. Supercomputer time was provided through the Leadership Resource Allocation MCB20012 on Frontera of the Texas Advanced Computing Center, the Extreme Science and Engineering Discovery Environment (XSEDE) allocation no. MCA05S028 and NSM PARAM Seva at IIT Hyderaband.

Keywords: Supramolecular chemistry · Foldamers · Organic nanotubes · Lithium channels · H-bonds

[1] a) E. Jakobsson, O. Argüello-Miranda, S. W. Chiu, Z. Fazal, J. Kruczek, S. Nunez-Corrales, S. Pandit, L. Pritchet, *J. Membr. Biol.* **2017**, *250*, 587-604; b) S. Puglisi-Allegra, S. Ruggieri, F. Fornai, *Transl Psychiatry.* **2021**, *11*, 366-366; c) A. J. Ferrari, A. J. Baxter, H. A. Whiteford, *J. Affect. Disord.* **2011**, *134*, 1-13; d) L. Bessonova, K. Ogden, M. J. Doane, A. K. O'Sullivan, M. Tohen, *Clinicoecon Outcomes Res.* **2020**, *12*, 481-497; e) M. Gitlin, *Int. J. Bipolar Disord.* **2016**, *4*, 27-27; f) E. Richelson, *Science* **1977**, *196*, 1001-1002; g) C. E. Naylor, C. Bagnéris, P. G. DeCaen, A. Sula, A. Scaglione, D. E. Clapham, B. A. Wallace, *Embo J.* **2016**, *35*, 820-830.

[2] a) U. Bardi, *Sustainability* **2010**, *2*, 980-992; b) C. Liu, Y. Li, D. Lin, P.-C. Hsu, B. Liu, G. Yan, T. Wu, Y. Cui, S. Chu, *Joule* **2020**, *4*, 1459-1469.

[3] S.-P. Zheng, L.-B. Huang, Z. Sun, M. Barboiu, *Angew. Chem. Int. Ed.* **2021**, *60*, 566-597.

[4] a) C. Lang, X. Deng, F. Yang, B. Yang, W. Wang, S. Qi, X. Zhang, C. Zhang, Z. Dong, J. Liu, *Angew. Chem. Int. Ed.* **2017**, *129*, 12842-12845; b) C. L. Ren, J. Shen, H. Q. Zeng, *J. Am. Chem. Soc.* **2017**, *139*, 12338–12341; c) M. Barboiu, *Acc. Chem. Res.* **2018**, *51*, 2711-2718; d) L. Z. Zeng, H. Zhang, T. Wang, T. Li, *Chem. Commun.* **2020**, *56*, 1211-1214; e) F. Chen, J. Shen, N. Li, A. Roy, R. J. Ye, C. L. Ren, H. Q. Zeng, *Angew. Chem. Int. Ed.* **2020**, *59*, 1440-1444; f) S. Qi, C. Zhang, H. Yu, J. Zhang, T. Yan, Z. Lin, B. Yang, Z. Dong, *J. Am. Chem. Soc.* **2021**, *143*, 3284-3288; g) D. Qiao, H. Joshi, H. Zhu, F. Wang, Y. Xu, J. Gao, F. Huang, A. Aksimentiev, J. Feng, *J. Am. Chem. Soc.* **2021**, *143*, 15975-15983; h) L. Jin, C. Sun, Z. Li, J. Shen, H. Q. Zeng, *Chem. Commun.* **2023**, *59*, 3610-3613; i) H. Zhang, R. Ye, Y. Mu, T. Li, H. Q. Zeng, *Nano Lett.* **2021**, *21*, 1384-1391.

[5] a) A. Nakano, Q. Xie, J. V. Mallen, L. Echegoyen, G. W. Gokel, *J. Am. Chem. Soc.* **1990**, *112*, 1287-1289; b) G. W. Gokel, A. Mukhopadhyay, *Chem. Soc. Rev.* **2001**, *30*, 274-286; c) F. Otis, C. Racine-Berthiaume, N. Voyer, *J. Am. Chem. Soc.* **2011**, *133*, 6481-6483.

[6] a) V. Gorteau, G. Bollot, J. Mareda, A. Perez-Velasco, S. Matile, *J. Am. Chem. Soc.* **2006**, *128*, 14788-14789; b) C. R. Yamnitz, S. Negin, I. A. Carasel, R. K. Winter, G. W. Gokel, *Chem. Commun.* **2010**, *46*, 2838-2840; c) A. Vargas Jentzsch, S. Matile, *J. Am. Chem. Soc.* **2013**, *135*, 5302-5303; d) T. Saha, A. Gautam, A. Mukherjee, M. Lahiri, P. Talukdar, *J. Am. Chem. Soc.* **2016**, *138*, 16443-16451; e) X. Wei, G. Zhang, Y. Shen, Y. Zhong, R. Liu, N. Yang, F. Y. Al-mkhaizim, M. A. Kline, L. He, M. Li, Z.-L. Lu, Z. Shao, B. Gong, *J. Am. Chem. Soc.* **2016**, *138*, 2749-2754; f) C. Ren, X. Ding, A. Roy, J. Shen, S. Zhou, F. Chen, S. F. Yau Li, H. Ren, Y. Y. Yang, H. Q. Zeng, *Chem. Sci.* **2018**, *9*, 4044-4051; g) C. L. Ren, F. Zeng, J. Shen, F. Chen, A. Roy, S. Y. Zhou, H. S. Ren, H. Q. Zeng, *J. Am. Chem. Soc.* **2018**, *140*, 8817–8826; h) W.-L. Huang, X.-D. Wang, Y.-F. Ao, Q.-Q. Wang, D.-X. Wang, *J. Am. Chem. Soc.* **2020**, *142*, 13273-13277; i) X. Wu, A. M. Gilchrist, P. A. Gale, *Chem* **2020**, *6*, 1296-1309; j) A. Mondal, S. N. Save, S. Sarkar, D. Mondal, J. Mondal, S. Sharma, P. Talukdar, *J. Am. Chem. Soc.* **2023**, *145*, 17, 9737-9745 .

[7] a) B. P. Benke, P. Aich, Y. Kim, K. L. Kim, M. R. Rohman, S. Hong, I.-C. Hwang, E. H. Lee, J. H. Roh, K. Kim, *J. Am. Chem. Soc.* **2017**, *139*, 7432-7435; b) L. Yuan, J. Shen, R. J. Ye, F. Chen, H. Q. Zeng, *Chem. Commun.* **2019**, *55*, 4797-4800; c) A. Roy, H. Joshi, R. J. Ye, J. Shen, F. Chen, A. Aksimentiev, H. Q. Zeng, *Angew. Chem. Int. Ed.* **2020**, *59*, 4806-4813.

[8] L. Yuan, P. Jiang, J. Hu, H. Q. Zeng, Y. Huo, Z. Li, H. Q. Zeng, *Chin. Chem. Lett.* **2022**, *33*, 2026-2030.

[9] a) J. Shen, R. Ye, Z. Liu, H. Q. Zeng, *Angew. Chem. Int. Ed.* **2022**, *61*, e202200259; b) T. Yan, S. Liu, J. Xu, H. Sun, S. Yu, J. Liu, *Nano Lett.* **2021**, *21*, 10462-10468.

[10] a) A. Roy, J. Shen, H. Joshi, W. Song, Y.-M. Tu, R. Chowdhury, R. Ye, N. Li, C. Ren, M. Kumar, A. Aksimentiev, H. Q. Zeng, *Nat. Nanotech.* **2021**, *16*, 911-917; b) J. Shen, A. Roy, H. Joshi, L. Samineni, R. J. Ye, Y.-M. Tu, W. Song, M. Skiles, M. Kumar, A. Aksimentiev, H. Q. Zeng, *Nano Lett.* **2022**, *22*, 4831–4838; c) W. Song, H. Joshi, R. Chowdhury, J. S. Najem, Y.-X. Shen, C. Lang, C. B. Henderson, Y.-M. Tu, M. Farell, M. E. Pitz, C. D. Maranas, P. S. Cremer, R. J. Hickey, S. A. Sarles, J.-I. Hou, A. Aksimentiev, M. Kumar, *Nat. Nanotech.* **2020**, *15*, 73-79; d) J. Shen, R. J. Ye, A. Romanies, A. Roy, F. Chen, C. L. Ren, Z. Liu, H. Q. Zeng, *J. Am. Chem. Soc.* **2020**, *142*, 10050–10058; e) Z.-J. Yan, D. Wang, Z. Ye,

T. Fan, G. Wu, L. Deng, L. Yang, B. Li, J. Liu, T. Ma, C. Dong, Z.-T. Li, L. Xiao, Y. Wang, W. Wang, J.-L. Hou, *J. Am. Chem. Soc.* **2020**, *142*, 15638-15643; f) W. Song, M. Kumar, *Langmuir* **2022**, *38*, 9085–9091; gh) L.-B. Huang, A. Hardiagon, I. Kocsis, C.-A. Jegu, M. Deleanu, A. Gilles, A. van der Lee, F. Sterpone, M. Baaden, M. Barboiu, *J. Am. Chem. Soc.* **2021**, *143*, 4224-4233.

[11] L. Zhang, C. Zhang, X. Dong, Z. Dong, *Angew. Chem. Int. Ed.* **2023**, *62*, e202214194.

[12] a) Y. Hamuro, S. J. Geib, A. D. Hamilton, *Angew. Chem., Int. Ed.* **1994**, *33*, 446; b) V. Berl, I. Huc, R. G. Khoury, M. J. Krische, J. M. Lehn, *Nature* **2000**, *407*, 720-723; c) J. Zhu, R. D. Parra, H. Q. Zeng, E. Skrzypczak-Jankun, X. C. Zeng, B. Gong, *J. Am. Chem. Soc.* **2000**, *122*, 4219-4220; d) B. Gong, *Chem.Eur. J.* **2001**, *7*, 4336-4342; e) D.-W. Zhang, X. Zhao, J.-L. Hou, Z.-T. Li, *Chem. Rev.* **2012**, *112*, 5271–5316; f) Y. P. Huo, H. Q. Zeng, *Acc. Chem. Res.* **2016**, *49*, 922-930; g) Y. Ferrand, I. Huc, *Acc. Chem. Res.* **2018**, *51*, 970-977; h) X. Hu, S. J. Dawson, P. K. Mandal, X. de Hatten, B. Baptiste, I. Huc, *Chem. Sci.* **2017**, *8*, 3741-3749; i) B. Gong, H. Q. Zeng, J. Zhu, L. H. Yuan, Y. H. Han, S. Z. Cheng, M. Furukawa, R. D. Parra, A. Y. Kovalevsky, J. L. Mills, E. Skrzypczak-Jankun, S. Martinovic, R. D. Smith, C. Zheng, T. Szyperski, X. C. Zeng, *Proc. Natl. Acad. Sci. U. S. A.* **2002**, *99*, 11583-11588.

[13] a) Y. Zhong, B. Kauffmann, W. Xu, Z.-L. Lu, Y. Ferrand, I. Huc, X. C. Zeng, R. Liu, B. Gong, *Org. Lett.* **2020**, *22*, 6938-6942; b) X. Li, T. Qi, K. Srinivas, S. Massip, V. Maurizot, I. Huc, *Org. Lett.* **2016**, *18*, 1044-1047; c) D.-W. Zhang, H. Wang, Z.-T. Li, *Macromol. Rapid Commun.* **2017**, *38*, 1700179.

[14] J. Shen, J. Fan, R. J. Ye, N. Li, Y. Mu, H. Q. Zeng, *Angew. Chem. Int. Ed.* **2020**, *59*, 13328-13334.

[15] C. Manske, M. Schmiedtchen, S. Gellhaar, M. Kiesel, J. Becker, *ACS Sustainable Chem. Eng.* **2022**, *10*, 5307-5314

[16] Du, X. K. Jiang, Z.-T. Li, *Tetrahedron Lett.* **2009**, *50*, 320-324

[17] a) J. C. Phillips, D. J. Hardy, J. D. Maia, J. E. Stone, J. V. Ribeiro, R. C. Bernardi, R. Buch, G. Fiorin, J. Hénin, W. Jiang, *J. Chem. Phys.* **2020**, *153*, 044130; b) J. Mahler, I. Persson, *Inorg. Chem.* **2012**, *51*, 425-438; c) Y. Sugita, A. Kitao, Y. Okamoto, *J. Chem. Phys.* **2000**, *113*, 6042-6051.

Entry for the Table of Contents

Artificial Lithium Channels

*Jie Shen, Deepa R, Zhongyan Li, Hyeonji Oh, Harekrushna Behera, Himanshu Joshi, Manish Kumar, Aleksei Aksimentiev and Huaqiang Zeng**

_____ ***Page – Page***

Sulfur-Containing Foldamer-Based Artificial Lithium Channels

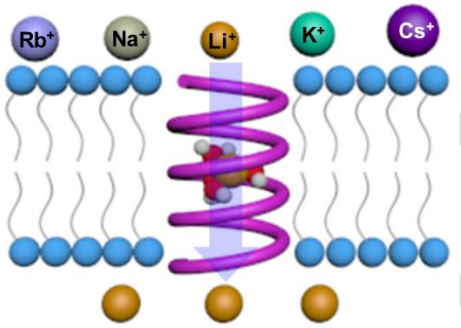

Using pivaloyl chloride as a mild one-pot copolymerization agent, we successfully constructed a novel class of sulfur-containing aromatic amide helices. Having an average height of 2.1 nm, 3.6 Å in cavity diameter and helically arranged S- and O-atoms along the inner wall, these nanotubes display highly selective and efficient transmembrane lithium transport, with transport selectivity factors of 15.3 and 19.9 over Na^+ and K^+ ions, respectively.